DRAFT VERSION SEPTEMBER 17, 2009
Preprint typeset using LaTeX style emulateapj v. 08/22/09

MSX VERSUS IRAS TWO-COLOR DIAGRAMS AND THE CSE-SEQUENCE OF OXYGEN-RICH LATE-TYPE STARS

LORÁNT O. SJOUWERMAN[1], STEPHANIE M. CAPEN[1, 2], MARK J. CLAUSSEN[1]

Draft version September 17, 2009

ABSTRACT

We present MSX two-color diagrams that can be used to characterize circumstellar environments of sources with good quality MSX colors in terms of IRAS color regions for oxygen-rich stars. With these diagrams we aim to provide a new tool that can be used to study circumstellar environments and to improve detection rates for targeted surveys for circumstellar maser emission similar to the IRAS two-color diagram. This new tool is especially useful for regions in the sky where IRAS was confused, in particular in the Galactic plane and bulge region. Unfortunately, using MSX colors alone does not allow to distinguish between carbon-rich and oxygen-rich objects. An application of this tool on 86 GHz SiO masers shows that for this type of masers an instantaneous detection rate of 60% to 80% can be achieved if target sources are selected according to MSX color (region).

Our investigations may have revealed an error in the MSX point source catalog version 2.3. That is, the photometry of the 21.3 μm (MSX E filter) band for most weak 8.28 μm (or MSX A filter) band sources seems off by about a factor two (0.5–1 magnitude too bright).

Subject headings: masers — catalogs — stars: AGB and post-AGB — circumstellar matter — stars: late-type — infrared: stars

1. INTRODUCTION

The two-color diagram (2CD) of stellar dust/gas envelope sources in the Infrared Astronomical Satellite (IRAS) point source catalog (PSC) has been very useful in characterizing the circumstellar environment of late-type stars, typically thought to be at the top of the Asymptotic Giant Branch (AGB) (Neugebauer et al. 1984; Beichman et al. 1985; Olnon et al. 1984; Hacking et al. 1985; van der Veen & Habing 1988). The IRAS 60μm/25μm versus 25μm/12μm two-color diagram statistically distinguishes between carbon-rich and oxygen-rich objects. In the latter color it also indicates the thickness of the circumstellar shell based on the appearance of the 9.7 μm silicate feature in the individual 7.7 to 22.6 μm low-resolution spectra (LRS) (Olnon et al. 1986; van der Veen & Habing 1988).

For many studies since the IRAS mission, the IRAS 2CD has thus been the starting point for color-selection of samples; not only to select AGB or Red Giant Branch (RGB) stars, but also to select e.g. proto-planetary nebulae, young stellar objects and starburst galaxies. The IRAS 2CD has been revolutionary in the study of the late evolutionary stages of evolved stars and chemical enrichment of the Galaxy due to the enhanced mass-loss of these stars. Moreover, the 2CD selection is very effective in finding circumstellar masers, and hence line-of-sight velocities of stars that then can be used for kinematic studies of the Galaxy. For example, objects in IRAS color region IIIb and IV (van der Veen & Habing 1988) have been targeted for 1612 MHz OH maser emission, whereas objects in region II usually have a circumstellar envelope (CSE) too thin to form and sustain these OH masers. On the other hand, objects in region II may be CSEs in which SiO maser emission is more likely to exist (e.g., Habing 1996, and the extensive list of references therein).

Electronic address: lsjouwerman@nrao.edu, stephanie.m.capen@enc.edu, mclaussen@nrao.edu
[1] National Radio Astronomy Observatory, P.O. Box O, Socorro, NM 87801
[2] Eastern Nazarene College, 23 East Elm Avenue, Quincy, MA 02170

The IRAS all-sky survey has a significant shortcoming in the sense that due to the low angular resolution, the Galactic plane (and in particular the bulge) survey region suffers from confusion. This is unfortunate as the majority of evolved stars (but also e.g. young stellar objects), are found in the plane. Therefore subsequent infrared surveys using the Infrared Space Observatory (ISO, with the ISOGAL survey), the Midcourse Space Experiment (MSX, with the Galactic Plane survey), and the Spitzer Space Telescope (with the GLIMPSE and MIPSGAL surveys) have concentrated on the Galactic plane and bulge with much better angular resolution[3] (Omont et al. 2003; Price et al. 2001; Benjamin et al. 2003; Carey et al. 2009). However, in correcting for IRAS' shortcoming, areas of the sky which overlap with the non-confused IRAS observations are minimal. Also, these other surveys have typically used other infrared wavebands and filters than IRAS. When the sources of interest are the intrinsically variable late-type stars, a direct comparison of colors between IRAS and e.g. MSX is, in principle, very difficult if not impossible.

Nevertheless, with the assumption that colors do not differ too much between observing epochs, i.e. stellar phase, and thus that results of a comparison between subsamples in a *statistical* sense can be interpreted, an attempt at a comparison between IRAS colors and other infrared colors can be made. Because the PSC of MIPSGAL and AKARI were not available in the summer of 2008 (when we began this study), and because ISOGAL and GLIMPSE were limited in spatial coverage and wavelength range respectively, we here present a comparison of IRAS and MSX colors. This comparison provides a tool to study, in the first instance, oxygen-rich AGB and RGB stars in MSX colors, similar to the IRAS 2CD. We note that the IRAS 2CD cannot fundamentally be replicated in MSX colors, because the MSX data do not extend to a long enough wavelength so that the vertical axis of the IRAS 2CD can be approximated with MSX data. Most of the analysis and discussion that follows concentrates on the horizontal extent of the IRAS 2CD.

[3] The AKARI mission is an all-sky survey (Murakami et al. 2007).

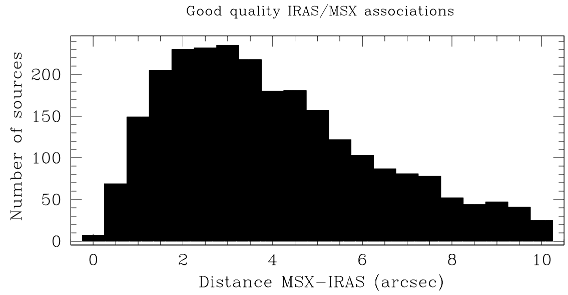

FIG. 1.— Positional offsets of the 2543 cross-identifications between the IRAS and MSX catalogs within 10″ radius using the van der Veen & Habing (1988) IRAS 2CD boundaries and with at least one good quality MSX color.

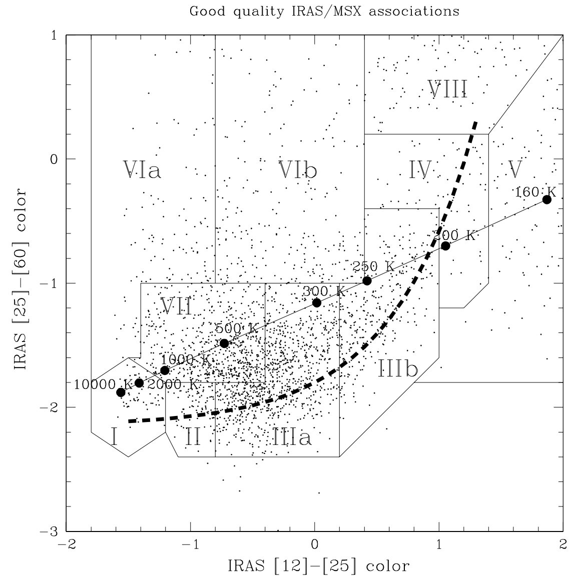

FIG. 2.— The "traditional" IRAS 2CD with uncorrected IRAS colors, color regions and color ranges as in van der Veen & Habing (1988, their Fig. 5b). The (solid) black body line, with temperature ticks, and the (dashed) "evolutionary track" are also shown. The "evolutionary track" is referred to as the "CSE-sequence" in the remainder of this paper. The data (points) are all 2543 good quality IRAS sources with a likely unique MSX counterpart within 10″ radius for which at least one good quality MSX color can be derived.

As an example of the capability of this comparison, we apply our MSX color tool to investigate the occurrence of 86 GHz SiO masers in color-selected sources in the Galactic bulge. It is our intention to derive similar comparisons for Spitzer (combined GLIMPSE and MIPSGAL) and AKARI colors once their point source catalogs are public, and to investigate the occurrence of other CSE masers as a function of color in a similar way using these new tools.

Section 2 describes the selection of the data sets; the sources that are in both the IRAS and MSX PSCs but excluding sources that could confuse or contaminate a statistical analysis. As most masers originate from oxygen-bearing molecules, we would like to be able to separate the carbon-rich from the oxygen-rich CSEs based purely on MSX colors. But before investigating such a separation in Sect. 3, we compare the "evolutionary curve" of oxygen-rich stars with circumstellar material in the IRAS 2CD as described by van der Veen & Habing (1988) with MSX colors. Note that this "evolutionary curve" is more a circumstellar envelope opacity measure than a strict stellar mass-loss evolution curve. Therefore we will refer to this curve as the "CSE-sequence" for oxygen-rich late-type stars in the remainder of this paper. The resulting MSX 2CDs are discussed in Sect. 4 and an example of their scientific usefulness is shown in Sect. 5. Future plans are collected in Sect. 6 before closing with a summary.

2. IRAS AND MSX DATA SELECTION

2.1. *Cross-identification between IRAS and MSX sources*

For the cross-identification between IRAS and MSX sources we used the positions from version 2.0 of the IRAS PSC (245889 sources) and Faint Source Catalog (FSC; 173044 sources) and version 2.3 from the MSX(6C) PSC (440487 sources) (Beichman et al. 1988; Egan et al. 2003).

Because we were very wary of contamination with incorrect cross-identifications, but on the other hand needed a data set of cross-identification as large as possible, we compromised between mission position accuracy and search radius. That is, IRAS PSC 12 μm positions typically are accurate to $\sim$ 7–9″, within a beam (angular resolution) of $\sim 1{\times}5'$, and MSX PSC 8.28 μm positions typically are accurate to $\sim$ 2″, within a beam of $\sim$ 18″ (Neugebauer et al. 1984; Hacking et al. 1985; Ojha et al. 2007; Beichman et al. 1988; Egan et al. 2003). We therefore used a search radius of 10″; the arithmetic mean of the beam and accuracy of the MSX mission, which is the more restrictive between IRAS and MSX. We used the same 10″ to cross-identify the MSX PSC with the IRAS FSC for two reasons. First, this expands the data set with more sources to compare IRAS and MSX colors. Second, it also reveals those IRAS-MSX PSC cross-identifications that could be confused with faint IRAS sources. Our data set thus excludes the MSX sources that had more than one possible IRAS counterpart within 10″, whether or not from the IRAS PSC or FSC, but also includes the (single) fainter IRAS counterparts. In total we found 45895 MSX sources identified with single IRAS PSC sources and 620 identified with single IRAS FSC sources (46515 total). Multiple identifications within 10″ were found for 482 MSX sources, whereas 393490 MSX sources had no counterpart in the IRAS PSC nor in the IRAS FSC within 10″ radius.

Two MSX sources were removed because they could be (at 6.64″ or 5.54″) identified with the same FSC source. Similarly, we removed another 76 MSX sources for which the identification with a unique IRAS PSC source within 10″ was ambiguous. To be consistent with the multiple identifications above, this means removing the MSX source even in the case where one possible identification was within 3″ (2.87″) and the other was as far as (almost) 10″ (9.60″) away. From this sub-total of 46437 sources which match in position, we removed 26743 cross-identifications for which the MSX sources had fewer than two reliable flux densities (i.e., "quality numbers" for the photometry which were not 3 or 4), i.e., for which not a single reliable, good quality MSX color could be calculated. Another 16194 IRAS sources were removed for which any of the 12, 25 or 60 μm fluxes were unreliable (quality not 3) as in that case we could not place them in the IRAS 2CD diagram reliably. Finally, another 957 sources were removed as they fall outside the traditional van der Veen & Habing (1988) IRAS 2CD color magnitude range limits (their Fig. 5a, 5b: $-2 < [12]-[25] < 2$ and $-3 < [25]-[60] < 1$; see next subsection). The remaining catalog of good quality IRAS sources in the traditional van der Veen & Habing (1988) IRAS 2CD with a likely unique MSX counterpart within 10″ radius for which at least one good quality MSX color could

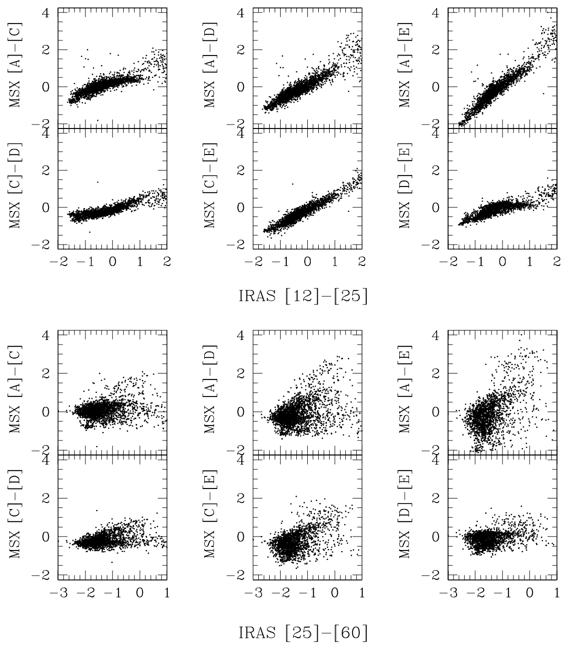

FIG. 3.— *Top:* uncorrected IRAS [12]–[25] color versus combinations of the uncorrected good quality MSX colors for the 2455 sources (2543 less 88 from IRAS region VIII) in Figs. 1, 2. For the MSX [A]–[D] color, the [A]–[E] color and the [C]–[E] color there is a good correspondence to the IRAS [12]–[25] color, with [A]–[E] having a larger color range (a bigger stretch, steepest slope: Table 1). *Bottom:* same for the IRAS [25]–[60] color, where no one-to-one correspondence between the IRAS [25]–[60] color can be deduced for any MSX color.

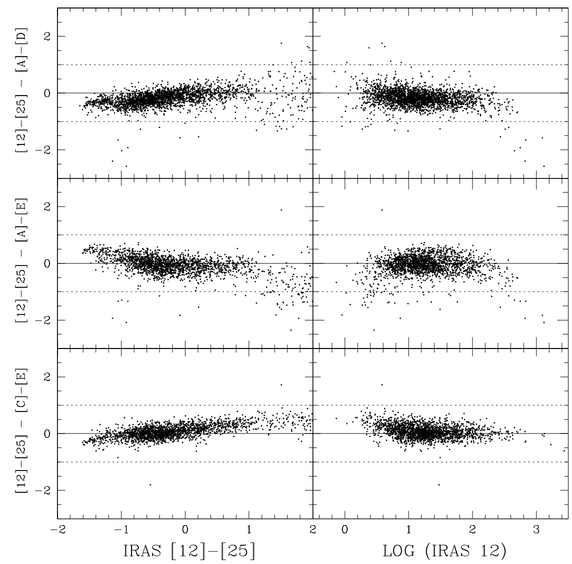

FIG. 4.— IRAS [12]–[25] color (*left*) and IRAS 12 μm flux (*right*) versus the difference between IRAS [12]–[25] color and MSX [A]–[D] color (*top*), MSX [A]–[E] color (*middle*) and MSX [C]–[E] color (*bottom*). The straight color differences are well within ± 1 magnitude (*dotted lines*). Table 2 fits the residual dependence on IRAS [12]–[25] color. The MSX color does not depend on total IRAS 12 μm flux density (neither is corrected for zero-magnitude offset). Results are similar for IRAS 25 and 60 μm flux densities (not shown). For very red sources, IRAS [12]–[25] > 1, only the MSX [C]–[E] color is closely related to the IRAS [12]–[25] color.

be derived is 2543. Only two sources are from the FSC. Figure 1 shows the histogram of the difference in position between the final 2543 IRAS and MSX associations. From the peaked distribution around 2.5$''$ (with $\sim 18''$ angular resolution) we conclude that the associations are very likely proper cross-identifications. The location of these remaining cross-identified IRAS/MSX sources in the IRAS 2CD diagram is shown in Fig. 2.

2.2. *Flux density and color definitions*

To be consistent with the original IRAS 2CD nomenclature we follow the (uncorrected) *color magnitude* definition used by van der Veen & Habing (1988), i.e. color magnitude $[\alpha]-[\beta] = -2.5 \times \log_{10}(F_\alpha/F_\beta)$ where F_χ is the measured flux density in Jansky (Jy) at waveband χ taken from the IRAS PSC/FSC version 2.0 or from the MSX PSC version 2.3 (Beichman et al. 1988; Egan et al. 2003). For IRAS wavebands we will use the numbers 12, 25 and 60 to designate the waveband; the center wavelength in μm of the filter passband. For MSX we will use the capital letters A, C, D and E for the wavebands centered at 8.28, 12.13, 14.65 and 21.3 μm respectively. If we call a source "blue" or "bluer" we refer to the smaller or more negative value(s) of a color; relatively larger or more positive color values are "red" or "redder". We also use the IRAS *color regions* determined by van der Veen & Habing (1988). That is, statistically, the oxygen-rich stars are located in the IRAS color regions identified with capital Roman numerals I, II, IIIa, IIIb, IV and V along the CSE-sequence, and carbon-rich stars typically are located in the IRAS color regions VIa, VIb and VII (Fig. 2). Color region VIII contains a complex mixture of sources. For the remainder of this paper we will concentrate on the oxygen-rich CSE-sequence I–V, completely ignore the 88 sources in color region VIII, and only occasionally comment on the carbon-rich sources in color regions VIa, VIb and VII. Later we will also introduce MSX color regions with non-capitalized Roman numerals (*i*, *ii*, *iiia*, *iiib*, *iv* and *v*) (to keep them recognizable as distinct MSX, rather than IRAS color regions), but where the same type of sources can be found in the different 2CDs (Sect. 4).

In our analysis we have chosen not to apply any zero-magnitude or color corrections. One of the strengths of the IRAS 2CD as defined by van der Veen & Habing (1988) is that it also did not have any of these corrections applied. The analysis of van der Veen & Habing (1988) was therefore independent of different choices of extinction curves and spectral energy distributions (SEDs) of individual objects. Only in Sect. 3.2 we will temporarily divert and apply a zero-magnitude correction – a simple axis shift – to compare our data with other data sets. The zero-magnitude correction is applied by, e.g., adding $2.5 \times \log_{10}(\frac{58.49}{18.29}) = 1.2622$ to the uncorrected [A]–[D] color and $2.5 \times \log_{10}(\frac{18.29}{8.80}) = 0.7943$ to the uncorrected [D]–[E] color, where 58.49, 26.51, 18.29 and 8.80 Jy are the zero-magnitude flux densities for the MSX bands A, C, D and E, respectively.

Finally, although we made an effort to exclude data that is "confused" (i.e., where the IRAS beam would include emission from several objects as compared to emission from a single object in the smaller MSX beam), it is quite possible that a few sources are confused or mis-identified. However, from the tail of Fig. 1 we estimate the number of mis-identifications or confused sources is less than 10%. Since we are making a statistical comparison of the colors, we expect no major difference in our conclusions when a few misidentified objects

TABLE 1
LEAST SQUARE FITS[a] OF IRAS [12]–[25] VERSUS MSX COLORS

MSX	slope	offset	RMS	MSX	slope	offset	RMS
[A]–[C]	0.468	0.230	0.224	[C]–[D]	0.375	–0.099	0.154
[A]–[D]	0.852	0.133	0.283	[C]–[E]	0.765	–0.100	0.177
[A]–[E]	1.227	0.140	0.296	[D]–[E]	0.384	0.003	0.205

[a]: MSX color = slope · (IRAS [12]–[25]) + offset

TABLE 2
LEAST SQUARE FITS OF IRAS/MSX COLOR DIFFERENCES

IRAS – MSX colors	slope	offset	RMS
(IRAS [12]–[25]) – (MSX [A]–[D])	0.148	–0.133	0.283
(IRAS [12]–[25]) – (MSX [A]–[E])	–0.227	–0.140	0.296
(IRAS [12]–[25]) – (MSX [C]–[E])	0.235	0.100	0.177

remain in the sample.

3. FROM IRAS COLORS TOWARD MSX COLORS

3.1. *The IRAS CSE-sequence in MSX Colors*

The CSE-sequence of oxygen-rich objects in the IRAS 2CD (see Fig. 2) is an exponential function of the IRAS [12]–[25] color resulting in an IRAS [25]–[60] color. With respect to the [12]–[25] color region domain the CSE-sequence overlaps in regions IIIb and IV (between $0.4 < [12]-[25] < 1.0$) and in regions IV and V (between $1.0 < [12]-[25] < 1.4$). However, this overlap is much less than in the [25]–[60] color region domain, where regions I–IIIb overlap between $-2.4 < [25]-[60] < -1.6$. It is therefore convenient to regard the CSE-sequence in terms of IRAS [12]–[25] color. Using the [12]–[25] colors at this stage does not distinguish between carbon-rich objects in regions VIa, VIb and VII and oxygen-rich objects along the CSE-sequence for $[12]–[25] < 0.4$; we will discuss this further in Sect. 3.2.

Strictly speaking, in terms of the center wavelength of the wavebands, the IRAS [12]–[25] color would correspond roughly to the MSX [C]–[E] color, with no corresponding color in the Spitzer (GLIMPSE+MIPS) nor in the ISOGAL surveys. However, as readily explained in Ortiz et al. (2005), the MSX A filter covers the 9.7 μm silicate feature, whereas the 11.3 μm SiC feature would appear in the MSX C filter; the IRAS 12 μm band filter includes both features[4]. As the silicate feature is typically the most prominent in the IRAS LRS, the IRAS [12]–[25] color may also, or better, correspond to the MSX [A]–[E] color. Figures 3 & 4 and Table 1 compare the IRAS colors to the MSX colors that could be derived from the cross-identifications. This comparison shows that the IRAS [12]–[25] color can generally be converted to MSX colors, most notably in the MSX [A]–[E] and [C]–[E] colors, but also with a reasonable color range in the MSX [A]–[D] color (Table 2). We note that there is no dependence on total flux density at any waveband (Fig. 4). Except for the [C]–[E] color, the dispersion and deviation from the trend is in general larger for very red sources, where $[12]–[25] > 1$, but overall the agreement is well within a third of a magnitude. We note that most of these sources are intrinsically variable evolved stars for which a difference in color due to non-simultaneous observations within a mission, or observing different stellar phases between the IRAS and MSX missions is reflected in this dispersion (Robitaille et al. 2007). No conversion can be made for the IRAS [25]–[60] color. This is not surprising as all MSX colors are determined for the SED shortward of 25 μm, and are largely insensitive to the SED and IRAS color longward of 25 μm wavelength.

For the oxygen-rich sources along the CSE-sequence, this close correspondence to the IRAS [12]–[25] color to three MSX colors is fortunate, as the CSE-sequence thus can be represented by the IRAS [12]–[25] color, and also by the MSX [A]–[E], [C]–[E] and [A]–[D] colors. We will thus assume that the small inaccuracies of converting IRAS colors using the linear relations in Table 1 remain within the noise of the whole sample of derived MSX colors. Then the IRAS CSE-sequence can be described as MSX CSE-sequences by substituting the IRAS [12]–[25] color with two different MSX colors in Eq. 2 of van der Veen & Habing (1988) for the range of valid IRAS [12]–[25] colors ($-1.5 < [12]–[25] < +1.3$). It follows that the IRAS [25]–[60] color can be eliminated by equating the right hand sides of the two equations obtained above. Rearrangement of the resulting equation yields the MSX CSE-sequences given in Table 3 (Sect. 4.1).

3.2. *Carbon-rich or oxygen-rich? The MSX "OC-index"*

In a statistical sense IRAS colors can be used to separate the carbon-rich sources from the oxygen-rich sources, as the carbon-rich CSEs typically reside in IRAS regions VIa, VIb and VII. However, when only MSX colors are available the separation of carbon-rich from oxygen-rich envelopes becomes more of a problem. Although other information is sometimes available upon which a clearer distinction between carbon-rich and oxygen-rich CSEs can be made, (e.g. *J*, *K* or *L* band 2MASS or DENIS flux densities, Suh et al. (2001); Lumsden et al. (2002); Suh (2007)), the challenge is to make such a distinction using only the data available within the MSX catalog (e.g., Lumsden et al. 2002; Sevenster 2002; Ortiz et al. 2005). In our view the most promising case is the data in Fig. 3 of Ortiz et al. (2005) which implicitly suggest that a first separation can be made. Ortiz et al. (2005) show that discriminating between C and O rich stars is better done using $K-[A]$ versus $[A]-[D]$ colors (their Fig. 2), but here we only use MSX colors and turn to their analysis of the zero-magnitude corrected MSX $[D]-[E]$ versus MSX $[A]-[D]$ color (their Fig 3). The samples in Ortiz et al. (2005) are well defined as the data from Loup et al. (1993) that they use are identified as carbon-rich stars and indeed typically, but not uniquely, populate IRAS color regions VIa, VIb and VII (Loup et al. 1993, their Fig. 3). Similarly, but vice versa for oxygen-rich stars in regions I–V, this reminds one that the IRAS boundary between carbon-rich and oxygen-rich color regions is not strict.

In Fig. 3 of Ortiz et al. (2005) the carbon-rich stars (filled squares) are mostly separated from the oxygen-rich OH/IR objects by the line $[A]-[D] = -2\cdot([D]-[E])+2.5$ using zero-magnitude corrected colors. This separator is the dotted line in our Fig. 5 and labeled "C vs O"[5]. Is it possible to use this empirical line to generally make the division between carbon-rich and oxygen-rich objects when the composition of the envelope is not known a-priori, e.g., such as in samples used in

[4] The Spitzer InfraRed Array Camera (IRAC) 8.0 μm filter excludes both, which could complicate recognizing the CSE-sequence using IRAC data.

[5] As an interesting side note, these are colors involving the MSX D filter, whereas in the previous section (3.1) we mentioned that the "carbon feature", the SiC line, appears in the MSX C filter. Plausible components with carbon-bearing molecules which could affect the flux density in the D filter are those of HCN and C_2H_2 at ~ 14 μm (see e.g., Blommaert et al. 2005).

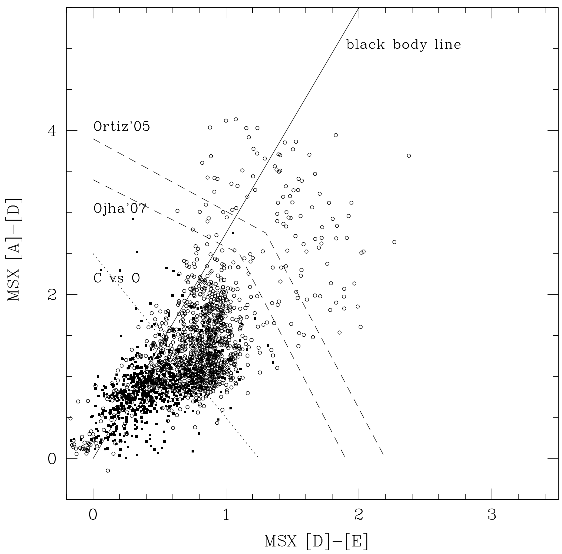

FIG. 5.— Zero-magnitude corrected MSX $[D]-[E]$ versus $[A]-[D]$ 2CD following Ortiz et al. (2005) (and Ojha et al. 2007) for the final selection of 2455 sources after removing those in IRAS color region VIII (88 sources). For 544 sources data could not be plotted in this diagram (see text). Filled squares are sources from IRAS color regions VIa, VIb and VII, the supposedly carbon-rich sources; open circles are supposedly oxygen-rich sources from IRAS color regions I–V. The dotted line labeled "C vs O" ($[A]-[D] = -2\cdot([D]-[E])+2.5$) is an empirical line derived from Fig. 3 in Ortiz et al. (2005). It suggests a division between carbon-rich and oxygen-rich sources in their data (see text and Fig. 6). Also drawn (dashed) are the lines from Ortiz et al. (2005) and Ojha et al. (2007) that depict a gap between stars and planetary nebulae or transition objects in their data; the gap is also apparent here. The (solid) black body temperature line ranges from 10,000 K at the origin to about 140 K at $[D]-[E] = 2$ (note that the black body temperature scale in Ortiz et al. (2005) is in error [R. Ortiz, priv. comm.]), crossing the "C vs O", "Ojha07"and "Ortiz05" line at T $\sim$ 400, 255 and 230 K respectively. These lines are roughly perpendicular to the black body temperature line and thus may be interpreted as temperature separators.

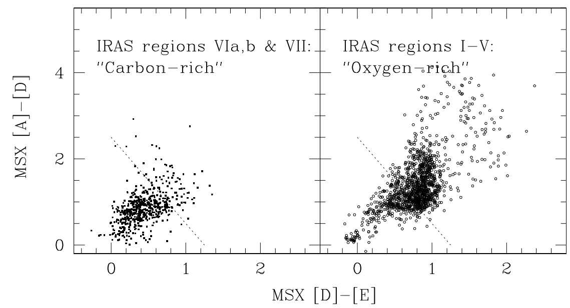

FIG. 6.— Zero-magnitude corrected MSX $[D]-[E]$ versus $[A]-[D]$ 2CD as Fig. 5, but now separated for IRAS color regions VIa, VIb and VII ("Carbon-rich"; 585 sources for which an "OC-index" could be calculated out of 966 sources in the carbon-rich IRAS regions VIa, VIb and VII) versus IRAS color regions I–V ("Oxygen-rich"; 1326 of 1489 sources). The (dotted) line is the empirical "C vs O" line from Fig. 5. Selecting sources to the lower left of the "C vs O" line, i.e., selecting sources for which the "OC-index" (Eq. 1) is less than zero (see text; Sect. 3.2), helps to increase the fraction of carbon-rich sources taken from the sample. However, selecting sources to the upper right, with a positive "OC-index", very effectively deselects oxygen-rich sources with T > 400 K (see Fig. 7).

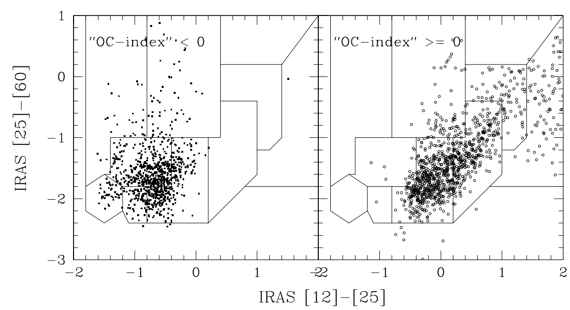

FIG. 7.— IRAS 2CDs of the 1911 sources separated according to the OC-index ("C vs O" line) for potentially carbon-rich objects (*left*; 886 sources) and oxygen-rich objects (*right*; 1025 sources). In general the division using the OC-index puts the sources in the expected IRAS regions, but the OC-index is not a good divider for sources hotter than 400 K (where the "C vs O" line crosses the black body temperature line in Fig. 5) as no oxygen-rich objects end up in IRAS regions I and II.

Ojha et al. (2007) and here?

In Fig. 5 the sources of our sample in IRAS color regions VIa, VIb and VII (filled squares) and the other regions (open circles) excluding region VIII (88 sources) seem to overlap in the densely populated part of the figure around the "C vs O" line. Note that only 1911 of the original 2455 sources could be plotted in this figure, as 544 sources are missing at least one good quality A, D, or E flux measurement. Figure 6 separates the two samples to show that supposed carbon-rich sources from IRAS region VIa, VIb and VII do appear in the oxygen-rich (top right) side of the "C vs O" dotted line. Supposed oxygen-rich sources also appear on the carbon-rich (bottom left) side. The IRAS color regions VIb and VII as described by van der Veen & Habing (1988) may still contain a large fraction of oxygen-rich stars based on the percentage of LRS classes 21–29 and 14–16 (Olnon et al. 1986) reported in the samples (van der Veen & Habing 1988). There is also some fraction of supposed oxygen-rich stars in regions II–IV which have LRS classes consistent with carbon-rich stars. This may also be seen, e.g., in Suh et al. (2001) where evolutionary models of carbon-rich stars do traverse oxygen-rich IRAS regions IIIa and IIIb, and models for oxygen-rich stars border region VII.

Not surprisingly this means that the IRAS region division between oxygen-rich and carbon-rich stars is not perfect. We therefore investigated whether a better separation between carbon-rich and oxygen-rich objects can be made using the MSX [D]–[E] versus [A]–[D] colors dividing at the "C vs O" line, with the understanding that the MSX separation may also not be perfect. We define the MSX "OC-index" for sources with good quality MSX A, D and E flux densities:

$$\mathrm{OC-index} \;=\; ([A]-[D]) \,+\, 2\cdot([D]-[E]) \,+\, \zeta \;, \qquad (1)$$

with $\zeta = -2.5$ for zero-magnitude corrected MSX colors and $\zeta = +0.35$ for uncorrected MSX colors. The OC-index is thus negative if the source is on the supposedly carbon-rich side of the "C vs O" line and positive on the supposedly oxygen-rich side.

Figure 7 shows the IRAS 2CD for the sample, divided according to the OC-index separately. Although the OC-index seems to generally divide the carbon-rich from the oxygen-rich objects, it mistakenly identifies potential oxygen-rich sources in IRAS regions I and II as carbon rich. It does select the cooler and thicker CSEs in IRAS color regions IIIa–V, but since we are interested in the full CSE-sequence, (including IRAS color regions I and II), using this division does not suit our needs in this context. We conclude that regardless of the potential to increase the fraction of carbon-rich sources in samples of hot objects (T $>$ 400 K, left of the border between region VII and IIIa), the OC-index is more a measure of temperature than CSE chemistry (Fig. 7).

The main interest in the present study is in the oxygen-rich sources along the CSE-sequence. As none of the MSX colors relates closely to the IRAS [25]–[60] color, it is expected that the carbon-rich and oxygen-rich sources overlap in MSX colors where the uncorrected IRAS [12]–[25] color is less than $\sim +0.4$, the farthest extent of IRAS color region VIb. To eliminate the pollution of an oxygen-rich sample along the CSE-sequence with likely carbon-rich sources in the MSX color samples, we therefore removed from our sample all sources from the carbon-rich IRAS color regions VIa, VIb and VII (and VIII). However, we did not remove the 388 sources with OC-index < 0 from the sample as this would eliminate *all* hot (T $>$ 400 K) oxygen-rich objects as well. Thus a reduced sample of 1489 sources with good MSX colors in the oxygen-rich IRAS regions was used in the remainder of this paper. Note that we chose to eliminate the likely carbon-rich sources. An option to introduce different symbol colors (see Fig. 8) would not add to clarity in the figures later on, whereas opting for symbol colors according to their IRAS [12]–[25] color, and thus mislabeling them as oxygen-rich sources, would just plot them on top of the distribution of oxygen-rich sources with the same symbol color. That is, leaving them out from the comparison of infrared colors of oxygen-rich sources seems proper and does not alter our conclusions.

4. MSX TWO-COLOR DIAGRAMS

Using the sample of 1489 generally oxygen-rich sources, MSX 2CDs were constructed. In an attempt to describe MSX regions that would correspond to IRAS regions, it is important to determine MSX 2CDs in which the different IRAS regions clearly separate one from another. As with the IRAS regions, some overlap of sources is expected and unavoidable with these statistical approaches. All possible combinations of MSX 2CDs were investigated. However, as can be deduced from the IRAS-MSX relations in Sect. 3.1 and Fig. 3, the MSX colors [A]–[D], [A]–[E], and [C]–[E], which have a slope larger than 0.5, are most useful. Furthermore, a color using the E-filter is the most distinctive as it gives the largest color range (but note Sect. 4.1.1). Also, because all MSX colors represent the IRAS [12]–[25] color, a more or less linear relation between any of these two MSX colors may be expected albeit with different absolute color ranges. In Fig. 8 these MSX 2CDs are shown with different source colors, depending in which IRAS color region the MSX source resides (see top right panel). In general the trend is along the CSE-sequence which is no surprise as the CSE-sequence, the black body temperature curve and the IRAS [12]–[25] color all align with the sequence of IRAS color regions I–V.

4.1. *MSX color regions and the CSE-sequence*

Figure 8 shows that sources from a particular IRAS region (a specific color) generally populate a confined region in the MSX 2CD diagrams. We therefore determined MSX 2CD color regions for sources with IRAS colors of color region I, II, etc. We will name the MSX region with sources from IRAS color region I, MSX color region *i* and similarly, e.g., sources from IRAS color region IIIb, MSX color region *iiib*, etc. Using our limited sample of 1489 sources total, we empirically determined approximate MSX color region boundaries as follows (Fig. 8):

$$\text{MSX } \boldsymbol{i} : \begin{cases} -2.0 \leq [\mathrm{A}]-[\mathrm{D}] < -0.9 & \text{or} \\ -3.0 \leq [\mathrm{A}]-[\mathrm{E}] < -1.5 & \text{or} \\ -2.0 \leq [\mathrm{C}]-[\mathrm{E}] < -1.1 & \end{cases}$$

$$\text{MSX } \boldsymbol{ii} : \begin{cases} -0.9 \leq [\mathrm{A}]-[\mathrm{D}] < -0.6 & \text{or} \\ -1.5 \leq [\mathrm{A}]-[\mathrm{E}] < -0.7 & \text{or} \\ -1.1 \leq [\mathrm{C}]-[\mathrm{E}] < -0.75 & \end{cases}$$

$$\text{MSX } \boldsymbol{iiia} : \begin{cases} -0.6 \leq [\mathrm{A}]-[\mathrm{D}] < +0.4 & \text{or} \\ -0.7 \leq [\mathrm{A}]-[\mathrm{E}] < +0.4 & \text{or} \\ -0.75 \leq [\mathrm{C}]-[\mathrm{E}] < +0.1 & \end{cases}$$

$$\text{MSX } \boldsymbol{iiib} : \begin{cases} +0.4 \leq [\mathrm{A}]-[\mathrm{D}] < +5.0 & \text{and} \\ +0.1 \leq [\mathrm{C}]-[\mathrm{E}] < +0.55 & \text{or} \\ 1.4\cdot([\mathrm{A}]-[\mathrm{E}]) - ([\mathrm{A}]-[\mathrm{D}]) < +0.8 & \text{and} \\ +0.4 \leq [\mathrm{A}]-[\mathrm{E}] < +1.1 & \text{or} \\ +0.1 \leq [\mathrm{C}]-[\mathrm{E}] < +0.55 & \end{cases}$$

$$\text{MSX } \boldsymbol{iv} : \begin{cases} +0.8 \leq 1.4\cdot([\mathrm{A}]-[\mathrm{E}]) - ([\mathrm{A}]-[\mathrm{D}]) < +1.3 & \text{and} \\ +0.4 \leq [\mathrm{A}]-[\mathrm{E}] < +7.0 & \text{or} \\ +0.55 \leq [\mathrm{C}]-[\mathrm{E}] < +1.0 & \end{cases}$$

$$\text{MSX } \boldsymbol{v} : \begin{cases} 1.4\cdot([\mathrm{A}]-[\mathrm{E}]) - ([\mathrm{A}]-[\mathrm{D}]) \geq +1.3 & \text{and} \\ +1.1 \leq [\mathrm{A}]-[\mathrm{E}] < +7.0 & \text{or} \\ +1.0 \leq [\mathrm{C}]-[\mathrm{E}] < +5.0 & \end{cases}$$

Two regions in the [A]–[E] versus [A]–[D] diagram (upper left panel in Fig. 8) are not accounted for in the above determination due to the lack of sources. The first region is for $1.1 < [\mathrm{A}]-[\mathrm{E}] < 7.0$ and with $1.4\cdot([\mathrm{A}]-[\mathrm{E}]) - ([\mathrm{A}]-[\mathrm{D}]) < +0.8$, where sources from either IRAS region IIIb and IV can be expected. Sources from either IRAS region IV and V can be expected between $+0.4 \leq [\mathrm{A}]-[\mathrm{E}] < 1.1$ and with $1.4\cdot([\mathrm{A}]-[\mathrm{E}]) - ([\mathrm{A}]-[\mathrm{D}]) > +1.3$.

We also included the beginning, zero and end points of the CSE-sequence in the MSX 2CDs. These are the locations of the crosses in the MSX 2CDs (Fig. 8) where IRAS [12]–[25] equals to -1.5 (labeled C), zero (labeled S) and $+1.3$ (labeled E). The full CSE-sequence is a straight line between these points and can be obtained by eliminating the [25]–[60] color from the CSE-sequence equation in van der Veen & Habing (1988, their Eq. 2), or simply by equating the expressions

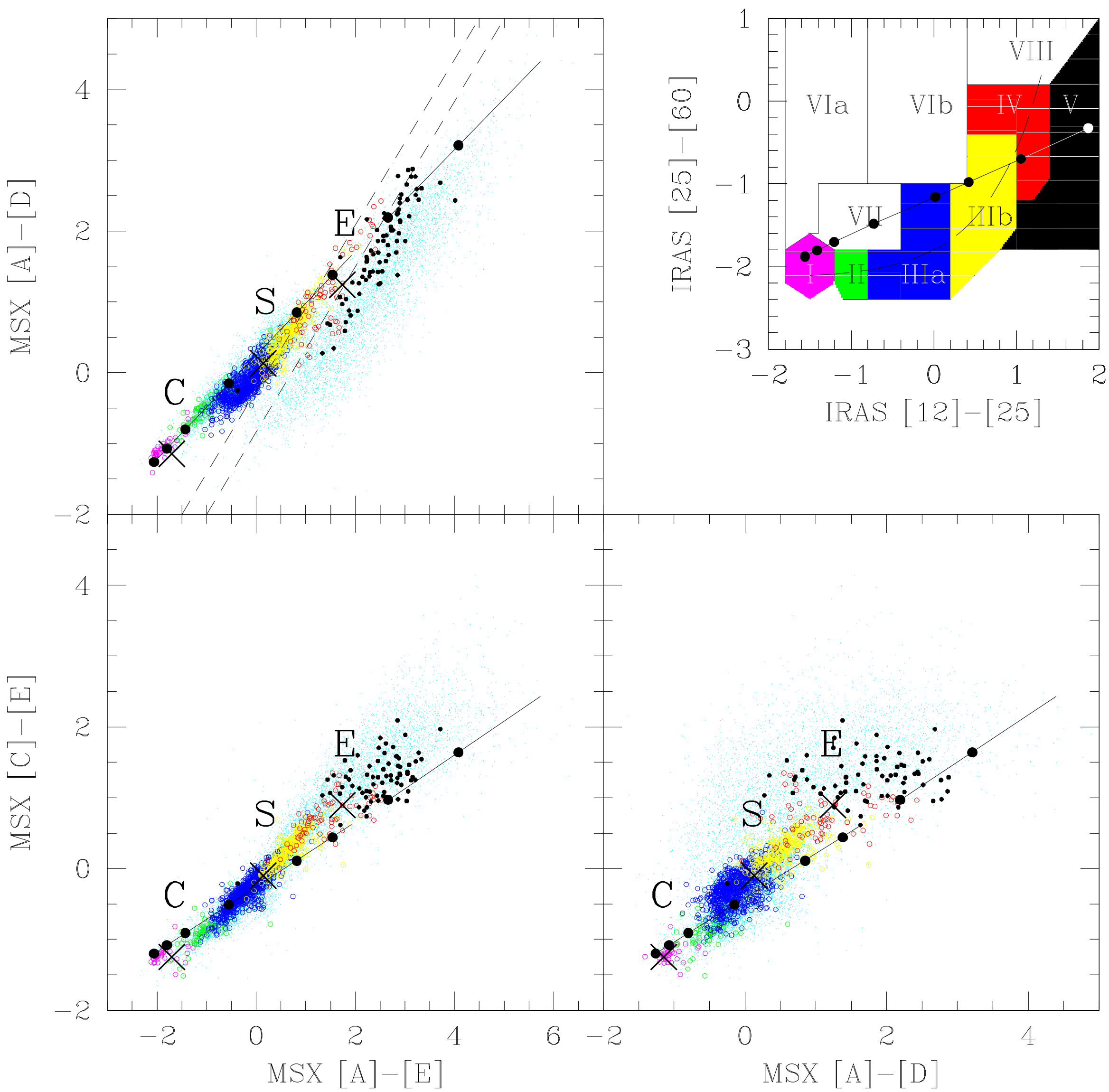

FIG. 8.— *Top right:* IRAS 2CD with color coded regions along the CSE-sequence. These color codes are used for the color of each source in the other panels, in the MSX 2CDs. For example, sources with IRAS colors consistent with being located in IRAS color region IIIb (yellow) appear in yellow in the MSX 2CDs. The black body temperature curve temperature labels are omitted at the ticks for clarity; they are the same as in Fig. 2, i.e., 10,000 K, 2000, 1000, 500, 300, 250, 200 and 160 K from left to right respectively. *Other panels:* MSX 2CDs of the 1489 sources in IRAS regions I–V. The color of the source depicts in which IRAS region it resides (see top right panel). Small cyan (lighter blue) points are sources with good MSX colors from the entire MSX catalog. The IRAS matches discussed here are a subset of mainly brighter sources which are in the Galactic plane. The CSE-sequence is the line connecting the crosses labeled C, S and E (the line itself is not drawn, for clarity), plotted at [12]–[25] = –1.5, 0 and +1.3 respectively. The solid line is the black body temperature curve starting at 10,000 K in the lower left, interrupted between 230 K and 200 K for reference, and ending at 130 K. The fat-dot ticks are at the same temperatures as in the IRAS 2CD. The dashed lines in the top left panel depict the lines separating sources from IRAS region IIIb from those from IRAS region IV and sources from region IV from those from IRAS region V – see text.

for [12]–[25] from Table 1 for different MSX colors over the [12]–[25] range in MSX colors where the CSE-sequence is defined. The expressions and color ranges for the CSE-sequence in MSX colors adapted here are given in Table 3. It can be seen that indeed the CSE-sequence starts in MSX color region *i*, has its zero point close to the border between regions *iiia* and *iiib*[6], and ends in region *iv*. It does not enter the region (*v*) with the reddest sources, which are mostly (proto-)planetary nebulae.

To obtain a subsample of sources that is characterized by colors of a certain IRAS color region, the selection criteria for the same (lower case) MSX color region can be directly applied if the parent sample contains uncorrected MSX colors. For example, a subsample of sources with CSEs resembling the IRAS IIIa region colors (blue in Fig. 8) can be drawn directly from the MSX catalog by applying one or more of

[6] In Fig. 8 the yellow symbols of region *iiib* overlap and unfortunately *overplot* the blue symbols of region *iiia*, making it unclear that the blue symbols continue under the yellow symbols. However, note that the yellow symbols do not extend much past the negative (lower left) side of [A]–[E] = 0.

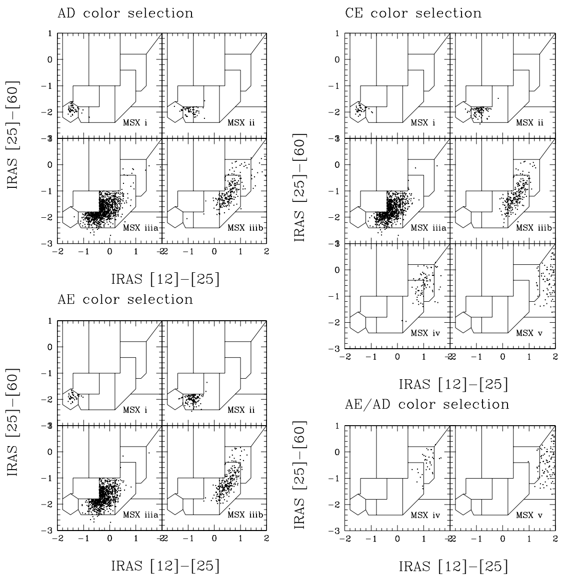

FIG. 9.— Resulting IRAS 2CD when the selection for MSX color regions is applied. IRAS color regions I, II and IIIa can readily be selected using a single MSX color, [A]–[D], [A]–[E] or [C]–[E]. Because the MSX [C]–[E] color corresponds best to the IRAS [12]–[25] color, IRAS color regions IIIb, IV and V can also be selected using the [C]–[E] color. If the [C]–[E] color is unavailable, due to a missing or unreliable C filter flux density, these regions can only be selected using a combination of the [A]–[D] and [A]–[E] colors.

the three equations for MSX region *iiia*. On the other hand, to obtain such a subsample from a parent sample that contains zero-magnitude corrected MSX colors, one would have to subtract the zero-flux magnitude fractions from Sect. 2.2 from the MSX source colors first[7]. As a reminder, we emphasize that carbon-rich sources in IRAS regions VIa, VIb and VII will overlap with MSX color regions *i*, *ii* and *iiia*, with a small tail in *iiib*–*v*. Using only MSX colors it is impossible to make an accurate estimate of the fraction of contamination with carbon-rich sources in a sample. However, to get an indication, in Table 4 we show the number of sources from the cross-identified IRAS/MSX data base (2543 sources; Sect. 2) in each IRAS color region, when sources are selected using any of the MSX selection rules above. It is apparent from this table that selecting a sample using the MSX color relations in general selects the sources with similar IRAS colors (e.g., MSX *iiia* and IRAS IIIa), but that also sources from nearby IRAS regions may fulfill the MSX selection rule. This, in a statistical approach, is not worrisome; e.g., using the MSX [A]–[D] color to select MSX *iiia* sources will yield 82% (816/995) of IRAS IIIa sources, provided that the sample is known to be mostly oxygen-rich along the CSE-sequence. Because of the degeneracy in the vertical axis of the IRAS 2CD when only MSX colors (or IRAS [12]–[25] colors) are available, the carbon-rich objects in IRAS regions VIa, VIb and VII also fulfill the MSX selection rules. The approximate number of sources in these IRAS regions (according to increasing [12]–[25] color) is also given in Table 4 per MSX selection rule. If the degeneracy between oxygen-rich and carbon-rich cannot be resolved, e.g. with the IRAS [25]–[60] color, then the *pure* fraction of IRAS region IIIa sources of

TABLE 3
CSE-SEQUENCE IN MSX TWO-COLOR DIAGRAMS (FIG. 8)

MSX CSE-sequence relations	Valid MSX CSE color ranges
[A]–[D] = 0.694 · ([A]–[E]) + 0.036	−1.145 < [A]–[D] < +1.241
[C]–[E] = 0.623 · ([A]–[E]) − 0.187	−1.701 < [A]–[E] < +1.735
[C]–[E] = 0.898 · ([A]–[D]) − 0.219	−1.248 < [C]–[E] < +0.895

the MSX *iiia* sources using the [A]–[D] color selection degrades to 50% (816/1624). Nevertheless, selecting on e.g. MSX *iiia* will thus indeed mostly yield IRAS IIIa sources, partly because some of the IRAS VIa, VIb and VII sources may be actually oxygen-rich since the IRAS boundaries also do not exactly separate the two populations. Because the density of carbon-rich sources is highest for [12]–[25] < 0, the highest contamination (cq. overlap) is in MSX color regions *i*, *ii* and *iiia*. For these regions other selection criteria to increase the oxygen-rich fraction are advisable (e.g. Messineo et al. (2002), Sect. 5). Again, the oxygen-rich and carbon-rich objects overlap around the dividing regions in the IRAS 2CD, in particular near IRAS region VII, so the numbers in Table 4 are indicative values only for any sample other than this IRAS/MSX cross correlated data set. For the particular example above, selecting MSX *iiia* sources using the [A]–[D] color, the fraction of oxygen-rich objects is 61% (995/1624). That is, for such a sample the remainder, 39%, may be carbon-rich and thus will not harbor SiO masers to begin with (Sect. 5).

4.1.1. *Possible error in MSX PSC 2.3 ?*

In our investigation we noticed possible error in the MSX PSC version 2.3 (Egan et al. 2003). In the MSX [A]–[E] versus [A]–[D] 2CD (the top left panel in Fig. 8) there seems to be a different distribution of sources which is shifted to the right and away from the CSE-sequence with respect to the main-populated area when *all* MSX sources with good quality photometry are used[8]. We could not account for this different distribution except by positing a somewhat different, redder population. In order to help confirm this possibility, we made the same 2CD diagram with data retrieved from MSX PSC version 1.2 (Egan et al. 1999). When compared to the PSC version 2.3 2CD there seems to be a more continuous distribution of redder (and weaker) objects in the diagram made from version 1.2 data (not shown).

From both versions of the PSC we selected objects with quality 3 or 4 in A, D, and E and constructed each color from the catalog data. Typically the sources weaker in flux density in the MSX A filter are affected, with a shift in [A]–[E] of ~ 0.5–1 magnitude redward. We understand that the difference between PSC versions 1.2 and 2.3 is that the photometry has been improved, and weaker sources have been included. However, we would not have expected the "gap" in the distribution of colors in the 2.3 data (top left panel in Fig. 8) that does not appear in the 1.2 data. The reason for this is currently unknown, but seems to originate from MSX E filter (21.3 μm band) fluxes that are a factor of about two too high for most of the weaker A filter (8.28 μm band) sources[9].

[7] Because the MSX A and D waveband filters are similar to the ISOGAL 7 and 15 μm waveband filters, selection on the zero-magnitude corrected ISOGAL [7]–[15] color ranges may appear to be similar to selection on the zero-magnitude color corrected MSX [A]–[D] color (Messineo et al. 2004).

[8] This may also be seen in the [A]–[D] versus [C]–[E] 2CD in the bottom right panel, where many sources show up above the main-populated area.

[9] A referee has explained the probable cause to be a combination of uncompensated variable response during the mission and the different techniques used for the extraction of the photometry in the different versions.

TABLE 4
CORRELATION MATRIX FOR SOURCES FOR WHICH THE MSX COLOR COULD BE CALCULATED AND FALL WITHIN THE RANGES OF THE EQUATIONS GIVEN IN SECT. 4.1 ("TOTAL"). THE NUMBERS ARE THE SOURCE COUNTS IN EACH IRAS COLOR REGION FOR EACH OF THE MSX COLOR SELECTION RULES, AND INDICATE THE POTENTIAL CONTAMINATION LEVEL OF OTHER SOURCES THAN TARGETED USING THE MSX RULES.

MSX color	IRAS CSE color region						Non-CSE IRAS region				Total	
selection used	I	II	IIIa	IIIb	IV	V	VIa	VII	VIb	VIII	I–V (O-rich)	I–VIII
MSX *i* using:												
[A]–[D]	48 (92%/27%)	3	1	-	-	-	52	71	1	-	52 (30%)	176
[A]–[E]	35 (90%/41%)	4	-	-	-	-	12	34	-	-	39 (46%)	85
[C]–[E]	35 (90%/37%)	4	-	-	-	-	10	46	-	-	39 (41%)	95
MSX *ii* using:												
[A]–[D]	6	29 (54%/12%)	19	-	-	-	32	137	17	-	54 (23%)	240
[A]–[E]	6	52 (50%/14%)	47	-	-	-	19	244	16	-	105 (27%)	384
[C]–[E]	6	48 (61%/17%)	25	-	-	-	17	183	10	-	79 (27%)	289
MSX *iiia* using:												
[A]–[D]	2	58	816 (82%/50%)	110	6	3	23	410	179	17	995 (61%)	1624
[A]–[E]	-	15	699 (90%/69%)	65	1	1	-	157	82	-	781 (77%)	1020
[C]–[E]	-	19	713 (88%/64%)	72	1	1	4	209	93	1	806 (72%)	1113
MSX *iiib* using:												
[A]–[D] & [C]–[E]	-	-	11	141 (83%/75%)	17	-	-	-	5	15	169 (89%)	189
[A]–[D] & [A]–[E]	-	-	31	203 (80%/68%)	20	-	-	2	19	24	254 (85%)	299
[C]–[E]	-	-	39	191 (77%/68%)	18	-	-	-	14	19	248 (88%)	281
MSX *iv* using:												
[A]–[D] & [A]–[E]	-	-	1	11	27 (64%/41%)	3	-	-	1	23	42 (64%)	66
[C]–[E]	-	-	1	29	41 (51%/36%)	9	-	-	1	32	80 (71%)	113
MSX *v* using:												
[A]–[D] & [A]–[E]	-	-	-	-	9	72 (89%/75%)	-	-	-	15	81 (84%)	96
[C]–[E]	-	-	-	-	10	60 (86%/73%)	-	1	-	11	70 (85%)	82

We have investigated whether our analysis also suffers from possible inaccuracies or effects in the weaker 8.28 μm objects. Fortunately the cross-identified objects, that are also detected by the less sensitive IRAS 12 μm detector, belong to the brighter MSX sample for which almost no sources are expected to be affected. This can also been seen from the lack of color-coded source symbols shifted to the right of the main distribution in the [A]–[E] versus [A]–[D] diagram. Note that the black dots of MSX color region *v* (or IRAS color region V, i.e., mostly planetary nebula) are shifted redward, because they are intrinsically redder than the CSE-sequence sources.

5. 86 GHZ SIO MASERS AND MSX COLOR

Previously the IRAS 2CD has been very successful in selecting objects to target: for example, for 1612 MHz maser emission (e.g., te Lintel Hekkert et al. 1991). Similarly, IRAS colors have been used to select targets for 86 GHz ($J = 2 \rightarrow 1, v = 1$) and 43 GHz ($J = 1 \rightarrow 0, v = 1$ and $v = 2$) SiO masers (e.g., Haikala 1990; Haikala et al. 1994; Nakada et al. 1993). Jiang et al. (1995) have made a careful analysis of the 43 GHz SiO maser detection rate as function of IRAS color and IRAS color region from the data collected by Izumiura et al. (1994, 1995a,b) in the Galactic bulge and disk. The Izumiura data were selected based on color *and* variability index with likely carbon-rich stars from IRAS regions VIa, VIb and VII removed.

In addition to an overall constant detection rate of SiO masers of about 61±3% as function of [12]–[25] color, Jiang et al. (1995) suggest that the detection rate in the Galactic bulge is higher than in the disk. Since in both the Galactic bulge and disk the IRAS survey suffered from confusion, the Jiang et al. (1995) study may have suffered from selection effects. It will be interesting to repeat this analysis based on MSX colors alone.

Another approach was used by Messineo et al. (2002) who bypassed the IRAS color selection and used the combined ISOGAL-DENIS data to empirically determine a complicated, extinction-corrected, color-magnitude-based selection from MSX [A]–[D] color and also on the MSX variability index in the Galactic bulge region. A cross-identification of Messineo et al. (2002)'s target sources with the IRAS PSC (10″ radius as in Sect. 2) results in only three sources with good photometry in all three IRAS bands, and only 81 with good photometry in [12]–[25] color. A selection based on IRAS color in this case would not have yielded an interesting sample, whereas the simple MSX tool presented here would have been extremely helpful in ease of use compared to their selection.

To assess their selection in terms of the [12]–[25] color analysis by Jiang et al. (1995), we plot the data from Messineo et al. (2002) in the MSX 2CDs in Fig. 10 and (non)-detection histograms in Fig. 11. Most sources selected by Messineo et al. (2002) are located in MSX region *iiia* which was the IRAS region they were targeting. Their sample likely includes more carbon-rich sources than the sample of Jiang et al. (1995) as Messineo et al. (2002) could not remove those sources using the IRAS [25]–[60] color.

The Messineo et al. (2002) 86 GHz SiO maser detection rate is consistent with an overall constant 65-66% as a function of either [A]–[D], [A]–[E] or [C]–[E] color, i.e., with (unavailable) [12]–[25] color (Fig. 11). Remarkably, this is the same result as Jiang et al. (1995) for the 43 GHz masers. For MSX region *iiia*, where the majority of the Messineo et al. (2002) sample lies, the IRAS/MSX cross-identified sam-

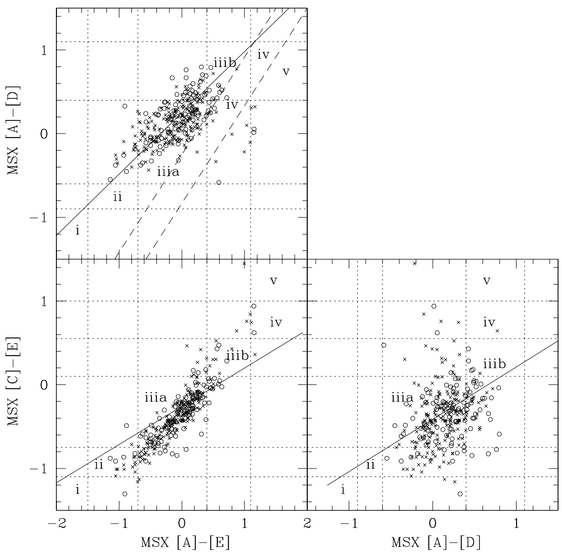

FIG. 10.— MSX 2CDs for 86 GHz SiO maser targets from Messineo et al. (2002). Crosses are detections, open circles are non-detections. Most sources selected by Messineo et al. (2002) are assigned to MSX color region *iiia*, comparable to the IRAS color region (IIIa) where for the Galactic bulge many SiO masers are expected (Jiang et al. 1995). Dotted horizontal and vertical lines show the MSX color region boundaries from Sect. 4.1. The other lines are as in Fig. 8.

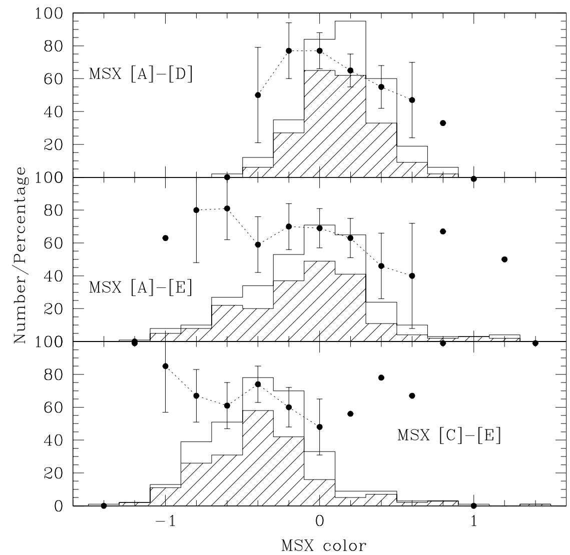

FIG. 11.— Detection rates as a function of MSX color for the SiO masers in Messineo et al. (2002). Shown are the histogram of targeted sources and the shaded histogram of the detected sources. The detection rate per 0.2 magnitude bin is depicted by dots, which are connected and have error bars only if the number of targets in the bin is ten or more. We note that the MSX photometry has changed slightly between PSC (preliminary) version 1.2 and version 2.3, so Messineo et al. (2002)'s strict [A]–[D] color selection, and the inclusion of ISOGAL selected sources, does not hold any more in our [A]–[D] color diagrams for some individual sources.

ple (Sect. 2) indicates that the carbon-star contamination is about 23–39%. Therefore, when selecting MSX *iiia* sources, using [A]–[D] colors (similar to the Messineo sample), we find 61% to be in the oxygen-rich region of the IRAS 2CD (see Table 4). Assuming that carbon-rich sources have all their oxygen locked up in carbon-monoxide molecules and thus never harbor SiO masers, this suggests that 1) almost all oxygen-rich sources selected using *iiia* would show detectable 86 GHz SiO maser emission, and 2) the complicated selection on [A]–[D] color by Messineo et al. (2002), which includes flux and variability information, was likely not much better than simply selecting on MSX color as they both yield very similar detection rates. As individual histogram bins at the blue (or red) end of the histograms in Fig. 11 typically indicate an 80% (or 50%) detection rate, there may be a small trend of decreasing SiO maser detection rate for redder sources. However, the range in MSX color is too small, and the uncertainties too large, to make a definite statement about this.

When compared to the MSX PSC 2.3, Messineo et al. (2002)'s list of targets resulted in 204 cross-identifications among the 271 SiO maser detections and 109 cross-identifications among the 173 targets without detected SiO maser emission[10]. The targets without cross-identifications must be targets that could only be selected using the more sensitive ISOGAL data – thus a sample of generally weaker infrared sources. As relatively more SiO maser detections are found in the brighter infrared MSX selection this probably confirms that brighter infrared sources are more likely to show detectable SiO maser emission (e.g., Messineo et al. 2002).

A more careful study can be done with a larger sample, using a larger color range. Here we have shown how such a sample selected on MSX colors (which are directly related to IRAS colors in the van der Veen & Habing (1988) 2CD) can be obtained quite easily compared to previous selections in areas where IRAS was confused.

6. POSSIBLE APPLICATIONS AND FUTURE PLANS

It should not be too difficult to find possible applications for this new tool. Almost any project using IRAS color region selection toward CSEs in regions on the sky where MSX data is superior to IRAS data can make use of this new tool. Moreover, particularly in the Galactic plane, new bulge and center projects can be attempted that were previously impossible because of the confusion in the IRAS data. For example, one should be able to find a population of (proto-)planetary nebulae hidden deeply in the nucleus of the Galaxy and study how their CSEs are affected by the more hostile local environment. Another example would be to select thousands of targets to survey for SiO maser emission in the Galactic plane. Such a survey would e.g. yield a map of Galactic rotation based on a few thousand point masses; gas is much more susceptible to non-gravitational forces. Stars and CSEs in regions too crowded for IRAS can be much better classified using MSX colors in terms of IRAS colors, etc. We leave it to the readers to find further applications in their own areas of expertise.

A straightforward future plan would be to compare and derive similar tools using the all-sky AKARI mission survey (formerly ASTRO-F; Murakami et al. 2007) with respect to the all-sky IRAS survey, but at much higher angular resolution. The AKARI PSC is expected to become available sometime after the summer of 2009. We have already commented on extending this study to the combined GLIMPSE and MIPSGAL data. We have begun to cross-identify the GLIMPSE and MSX PSCs, but the MIPSGAL (24 μm) PSC needed to obtain Spitzer data longward of 8 μm has been unfortunately delayed beyond the original release date.

[10] Instead of the 313 total sources here, Messineo et al. (2004) found 379 cross-identifications total within 15$''$ radius using MSX PSC version 1.2.

7. SUMMARY

Using cross-identifications between the IRAS and MSX source catalogs we have derived color ranges and color regions in MSX 2CDs that correspond to color regions along the "evolutionary track" or the CSE-sequence in the IRAS 2CD. Oxygen-rich objects in MSX color regions *i*, *ii*, *iiia*, *iiib*, *iv* and *v* can be expected to have similar CSEs and CSE properties as oxygen-rich objects in IRAS color regions I, II, IIIa, IIIb, IV and V, respectively. This tool should be useful in selecting sources with different CSEs, especially in regions where selection using IRAS data is unsatisfactory such as the (IRAS) confused Galactic bulge and plane regions.

However, it is impossible to distinguish between carbon-rich and oxygen-rich sources based on MSX colors alone; e.g. IRAS or near-infrared K and/or L band data is needed for that. This means that when only considering MSX colors, carbon-rich objects and oxygen-rich objects populate the same MSX regions, in particular *i*, *ii* and *iiia*. Selecting sources with a negative OC-index will increase the fraction of carbon-rich objects, but also deselect the low (T $<$ 400 K) temperature carbon-rich objects. The reverse selection is not likely: that one increases the fraction of oxygen-rich objects in a sample by selecting sources with positive OC-index, unless only cool sources are considered.

We also seem to have revealed an error in the photometry of the MSX E filter band. The flux density seems a factor ~ 2 too high, or ~ 0.5–1 magnitude too bright in [E], for weak A filter band sources in the MSX point source catalog version 2.3. This error does not seem to be evident in MSX PSC version 1.2, which has a smaller number of weak sources. The reason for this discrepancy is probably due to the band E detector and a different handling of the photometry.

ACKNOWLEDGMENTS

We thank Maria Messineo and Roberto Ortiz for providing data, insight and healthy discussions. SMC acknowledges support from the "Research Experiences for Undergraduates" program, which is funded by the National Science Foundation. The National Radio Astronomy Observatory is a facility of the National Science Foundation operated under cooperative agreement by Associated Universities, Inc.

Facilities: IRAS (), MSX ()

REFERENCES

Beichman, C. A., Chester, T. J., Gautier, T. N., Helou, G., Oken, C., Raimond, E., Soifer, B. T., & Walker, D. 1985, Infrared Astronomy Satellite (IRAS) Catalogs and Atlases,
Beichman, C. A., Neugebauer, G., Habing, H. J., Clegg, P. E., & Chester, T. J. 1988, Infrared astronomical satellite (IRAS) catalogs and atlases. Volume 1: Explanatory supplement, 1
Benjamin, R. A., et al. 2003, PASP, 115, 953
Blommaert, J. A. D. L., Cami, J., Szczerba, R., & Barlow, M. J. 2005, Space Science Reviews, 119, 215
Carey, S. J. et al. 2009, PASP121, 76
Egan M. P., et al.(1999) "The Midcourse Space Experiment Point Source Catalog, Version 1.2 (June 1999)", Air Force Research Laboratory Technical Report AFRL-VS-TR-1999-1522
Egan M. P., et al.(2003) "The Midcourse Space Experiment Point Source Catalog, Version 2.3 (October 2003)", Air Force Research Laboratory Technical Report AFRL-VS-TR-2003-1589
Habing, H. J. 1996, A&A Rev., 7, 97
Hacking, P., et al. 1985, PASP, 97, 616
Haikala, L. K. 1990, A&AS, 85, 875
Haikala, L. K., Nyman, L.-A., & Forsstroem, V. 1994, A&AS, 103, 107
Izumiura, H., Deguchi, S., Hashimoto, O., Nakada, Y., Onaka, T., Ono, T., Ukita, N., & Yamamura, I. 1994, ApJ, 437, 419
Izumiura, H., et al. 1995a, ApJS, 98, 271
Izumiura, H., Deguchi, S., Hashimoto, O., Nakada, Y., Onaka, T., Ono, T., Ukita, N., & Yamamura, I. 1995b, ApJ, 453, 837
Jiang, B. W., Deguchi, S., Izumiura, H., Nakada, Y., & Yamamura, I. 1995, PASJ, 47, 815
Loup, C., Forveille, T., Omont, A., & Paul, J. F. 1993, A&AS, 99, 291
Lumsden, S. L., Hoare, M. G., Oudmaijer, R. D., & Richards, D. 2002, MNRAS, 336, 621
Messineo, M., Habing, H. J., Sjouwerman, L. O., Omont, A., & Menten, K. M. 2002, A&A, 393, 115
Messineo, M., Habing, H. J., Menten, K. M., Omont, A., & Sjouwerman, L. O. 2004, A&A, 418, 103
Murakami, H., et al. 2007, PASJ, 59, 369
Nakada, Y., Onaka, T., Yamamura, I., Deguchi, S., Ukita, N., & Izumiura, H. 1993, PASJ, 45, 179
Neugebauer, G., et al. 1984, ApJ, 278, L1
Ojha, D. K., Tej, A., Schultheis, M., Omont, A., & Schuller, F. 2007, MNRAS, 381, 1219
Olnon, F. M., Habing, H. J., Baud, B., Pottasch, S. R., de Jong, T., & Harris, S. 1984, ApJ, 278, L41
Olnon, F. M., et al. 1986, A&AS, 65, 607
Omont, A., et al. 2003, A&A, 403, 975
Ortiz, R., Lorenz-Martins, S., Maciel, W. J., & Rangel, E. M. 2005, A&A, 431, 565
Price, S. D., Egan, M. P., Carey, S. J., Mizuno, D. R., & Kuchar, T. A. 2001, AJ, 121, 2819
Robitaille, T. P., Cohen, M., Whitney, B. A., Meade, M., Babler, B., Indebetouw, R., & Churchwell, E. 2007, AJ, 134, 2099
Sevenster, M. N. 2002, AJ, 123, 2772
Suh, K.-W., Lee, J. W., & Kim, H.-Y. 2001, Journal of Astronomy and Space Sciences, 18, 15
Suh, K.-W. 2007, Journal of Astronomy and Space Sciences, 24, 197
te Lintel Hekkert, P., Caswell, J. L., Habing, H. J., Haynes, R. F., & Norris, R. P. 1991, A&AS, 90, 327
van der Veen, W. E. C. J., & Habing, H. J. 1988, A&A, 194, 125